Hindawi
Journal of Nanomaterials
Volume 2020, Article ID 4745726, 11 pages
https://doi.org/10.1155/2020/4745726

Research Article

Fabrication of TiO_2 Nanotube by Electrochemical Anodization: Toward Photocatalytic Application

O. Zakir,[1,2] **R. Idouhli**,[1] **M. Elyaagoubi**,[2] **M. Khadiri**,[1] **A. Aityoub**,[1] **Y. Koumya**,[1] **S. Rafqah**,[3] **A. Abouelfida**,[1] **and A. Outzourhit**[2]

[1]*Laboratory of Applied Chemistry and Biomass, Department of Chemistry, University Cadi Ayyad, Faculty of Science Semlalia, BP 2390 Marrakech, Morocco*
[2]*Laboratory of Nanomateriels for Energy and Environment, Department of Physics, University Cadi Ayyad, Faculty of Science Semlalia, BP 2390 Marrakech, Morocco*
[3]*Laboratoire de Chimie Analytique et Moléculaire, Faculté Polydisciplinaire de Safi, Université Cadi Ayyad, Safi, Morocco*

Correspondence should be addressed to O. Zakir; othmane.zakir@gmail.com

Received 13 July 2020; Revised 28 November 2020; Accepted 6 December 2020; Published 29 December 2020

Academic Editor: Miguel A. Correa Duarte

In this study, a self-organized nanotubular titanium dioxide (TiO_2) array was successfully produced by anodizing pure titanium in a mixture of glycerol, distilled water (8% vol.), and ammonium fluoride using a dual electrode system. The size control and distribution of the nanopores were performed in a DC voltage range varying from 30 V to 60 V. The diameter of TiO_2 nanopores varies from 59 to 128 nm depending on the anodizing voltage. Energy-dispersive X-ray spectroscopy (EDX) analysis reveals that the as-prepared films are essentially composed of TiO_2. According to the X-ray diffraction (XRD) and Raman spectroscopy analysis, the nanotubular arrays of TiO_2 annealed at 600°C for 2 hours are composed of a phase mixture of anatase and rutile. Mott-Schottky analysis showed that the TiO_2 nanotubes are consistent with an n-type semiconductor with a donor density of about 10^{17} cm^{-3}. Preliminary results on the photocatalytic degradation of a pharmaceutical pollutant showed that the TiO_2 nanotubes can be used as a promising material for application in wastewater treatment.

1. Introduction

Recently, owing to the diverse application of titanium dioxide TiO_2, a thorough research and experiments have been devoted to the preparation of titanium dioxide TiO_2 and the considerable number of parameters determining its formation. There is a vast amount of literature on the titanium dioxide application such as photoelectrochemical water splitting [1], water [2, 3] and air purification [4], solar energy conversion [5], medical applications [6], gas sensors [7], and supercapacitors [8]. These applications rely on the specific semiconductor nature of TiO_2, in particular anatase, which is an n-type semiconductor with a large band gap of about 3.2 eV [9].

In the last years, several techniques have received considerable attention for elaborating TiO_2 nanostructures with promising properties. The most often used methods include the sol-gel process [10, 11], the electrochemical anodization of titanium [12], the hydrothermal method [13], and sputtering [14]. Among these methods, titanium anodization is the most effective way to produce highly ordered nanoporous TiO_2 films [15]. It has been now demonstrated that two types of TiO_2 morphology can be obtained by electrochemical anodization: compact TiO_2 films are generally obtained in fluoride free electrolytes, whereas porous films can be prepared in electrolytes containing fluoride ions [16, 17].

The nanostructure of the pores on the titanium surface obtained by electrochemical anodization is strongly affected by several parameters, such as applied potential [12, 18, 19], anodization bath temperature [20], electrolyte composition [21], anodizing time [12, 19, 22], water content in the electrolyte [23, 24], and the fluoride ion concentration [19, 21, 25].

Considerable attention has been directed to study the mechanism of formation of nanotubular TiO_2 films by

electrochemical anodization. Consequently, a number of theories based on field dissolution [26] and localized acidification at the pore bottom that increases chemical dissolution [27, 28] have been proposed to explain some aspects of the mechanism related to the TiO_2 nanotube formation and growth.

The synthesis and properties of one-dimensional tubular arrays have been widely investigated. Lockman et al. [18] reported that in a mixture of Na_2SO_4 (1 M) and 5 wt% NH_4F, the diameters and lengths of the nanotubes increased with increasing anodization voltage from 10 V to 25 V and the average diameters of the nanotubes were about 80 nm, 70 nm, and 50 nm for anodization voltages of 20 V, 15 V and 12 V, respectively. Albu et al. [29] showed that the geometry of the nanotubular layer depends strongly on the applied potential and the fluoride concentration. However, Kulkarni et al. [24] studied the effect of anodization parameters on the morphology of the TiO_2 nanostructure and the mechanism converting the as-formed nanopores to nanotubes.

Very little work has been carried out on the anodization of titanium in glycerol. Indeed, Sreekantan et al. [30] have stipulated that in glycerol containing 6 wt% of ethylene glycol (EG) and 5 wt% NH_4F, in the voltage range from 20 to 60 V, the uniform TiO_2 nanotubes were reached with a voltage less than 30 V. For a potential up to 50 V, the structure of the anodized titanium tended to be irregular.

This work reports on the effect of anodization voltage on the morphology of nanotubular TiO_2 on the pure titanium surface and their electrochemical, structural, optical, and electrical properties. Different approaches are thoroughly investigated with the aim of producing a nanotubular titanium dioxide including current time transients, SEM along with EDX, X-ray diffraction, Raman spectroscopy, and impedance measurements.

2. Experimental

2.1. Chemicals. Titanium foil (99.99% pure, 2 mm thick), glycerol (99.8%, anhydrous), ammonium fluoride (98%), acetic acid (99.98%), HF (40%), H_2SO_4 (96%), and carbamazepine (99% purity) were purchased from Sigma-Aldrich (St-Louis, USA).

2.2. Elaboration and Characterization. To obtain reliable and reproducible results, the pure titanium sample underwent, before each test, a pretreatment consisting of polishing the electrode surface with an increasingly fine grade emery paper (SiC #400, #1200, #2000, and #4000), followed by rinsing with distilled water and then drying under airflow.

Afterwards, the sample was electrolytically polished in a solution containing hydrofluoric acid (18% *v*/*v*), sulfuric acid (40% *v*/*v*), and acetic acid (42% *v*/*v*) at a voltage of 11 V for 30 s. Samples are then abundantly rinsed with distilled water.

The anodization of pure titanium foils was carried out in an electrolytic bath consisting of a mixture of glycerol-distilled water (92 : 8% *v*/*v*) and ammonium fluoride (0.4 M) for 60 min, at a voltage ranging from 30 to 60 V, using a two-electrode cell with the titanium sample as the anode and a platinum electrode as the counter electrode.

Later with the intention of enhancing the crystallinity of as-synthesized nanoporous TiO_2 films, the anodized samples were annealed in a muffle furnace at 600°C for two hours with a heating ramp of 10°C/min.

The electrochemical study was performed in a 0.1 M Na_2SO_4 solution using a conventional three-electrode cell consisting of an anodized TiO_2 as the working electrode (WE), a saturated calomel electrode (SCE) as the reference electrode, and a platinum sheet (4 cm^2) as the counter electrode [31]. The measurements were performed using a VoltaLab potentiostat (PGZ301) controlled by the VoltaMaster 4 software. To perform the EIS experiments at steady state, the rotational speed of the stirrer was set at 200 rpm. The temperature was controlled in jacketed glass at 293 K using a bath thermostat (±1°C). The Mott-Schottky (MS) analysis was performed at a frequency of 1 kHz in wide voltage range (from -1 V to 1 V/SCE).

The morphology of the anodized samples and the elemental composition of the oxide films are examined by scanning electron microscopy (SEM) along with energy-dispersive X-ray spectroscopy (EDX). The crystal structure of the oxide films was determined by X-ray diffraction (XRD) (Rigaku, SmartLab SE, Cu Kα1, $\lambda = 1.5418$ Å) and Raman spectroscopy (Confotec MR520) with laser of wavelength $\lambda = 532$ nm. Pore diameter measurement is performed using the image processing software ImageJ.

The irradiation system used is equipped with an Ultra-Vitalux lamp at 300 W with high-pressure tungsten filament. A double-jacketed glass reactor allowed maintaining the temperature at 25°C of the solution during the irradiation time.

3. Results and Discussion

3.1. Current Time Transient Measurements. During the anodizing process, the variation of the current density as a function of time is monitored. Figure 1 shows the anodizing current density/time curves during the anodization at different potentials. The observed transients share similar trends. Three stages are typically observed in these curves related to the typical current density-time curve of the porous oxide formed under constant voltage. The kinetic trend consists of an initial fast drop (stage A), a steady increase (stage B), and a quasisteady state current density (stage C).

At stage A, the anodizing process begins, and the current quickly decreases to a minimum value because of the formation of a high resistance compact oxide layer on the surface by the interaction of the Ti^{4+} ions with the oxygen O^{2-} ions in the electrolyte according to the following reaction [32]:

$$Ti + 2H_2O \rightarrow TiO_2 + 4e^- + 4H^+ \quad (1)$$

At stage B, the current subsequently rises to a maximum as the pore formation progresses. This is due to the chemical dissolution of the oxide layer by fluoride ions that is

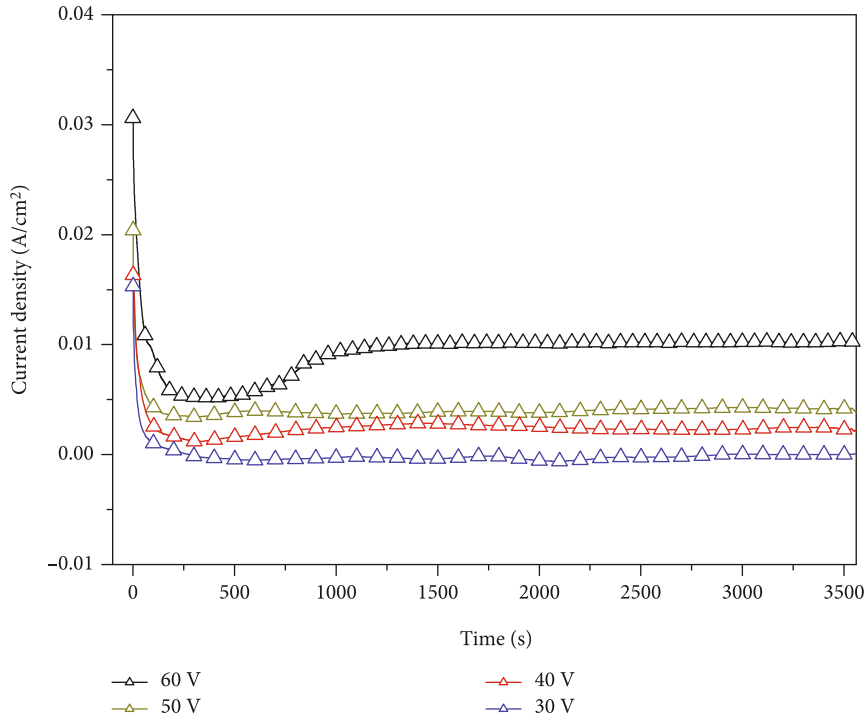

Figure 1: Current density/time curves obtained at different anodization potentials.

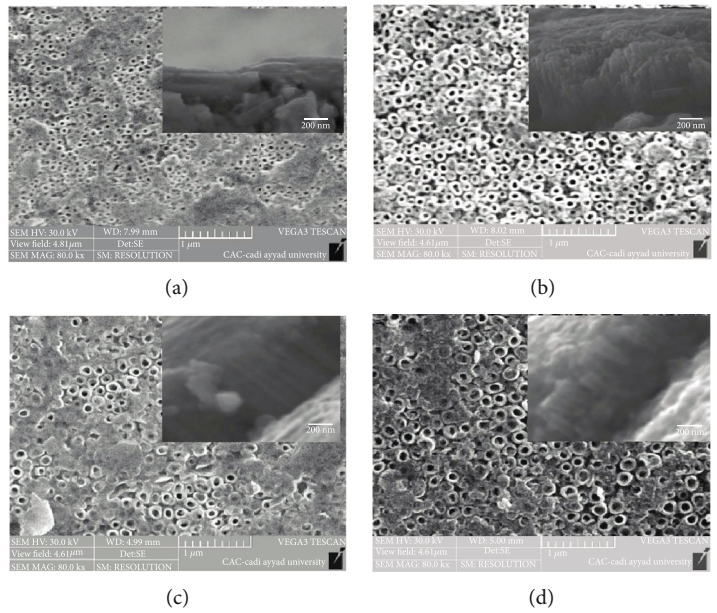

Figure 2: SEM top images and cross-sections of nanotube layers grown in glycerol-distilled water (92 : 8% *v*/*v*) and NH_4F (0.4 M) for 60 min at different anodizing potentials: (a) 30 V, (b) 40 V, (c) 50 V, and (d) 60 V.

promoted by an electric field created between the cell electrodes. Small pits are formed on the surface of the compact layer followed by the formation of a nanoporous structure according to the following reaction [32, 33]:

$$TiO_2 + 6F^- + 4H^+ \rightarrow TiF_6^- + 2H_2O \quad (2)$$

At the final stage, the current density attains a constant value when a steady state is reached owing to the formation of TiO_2 nanotubes [34].

3.2. Morphological and Composition Characterization. For the morphological analysis of TiO_2 nanotubular layers formed on the titanium substrate at different potentials, a

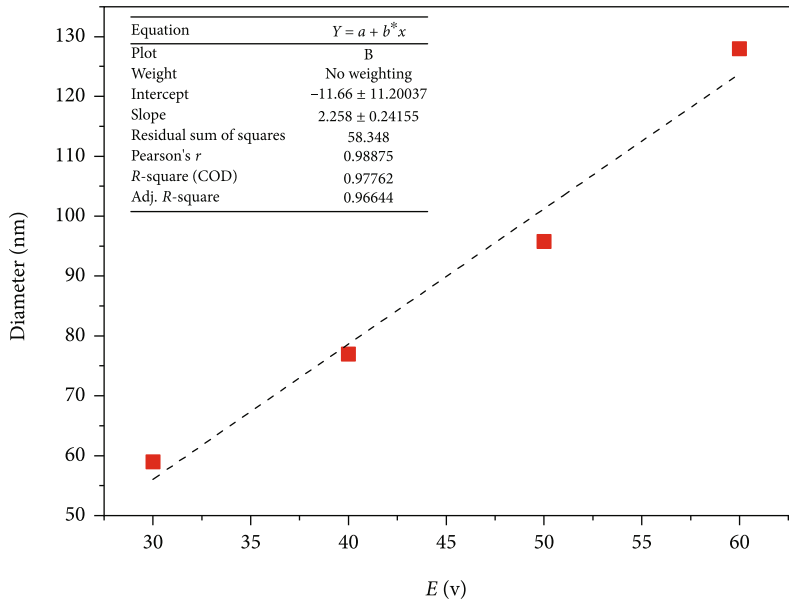

Figure 3: The variation of the TiO_2 nanotube diameters as a function of the anodizing voltage for 60 minutes in glycerol-distilled water (92 : 8% *v*/*v*) and NH_4F (0.4 M).

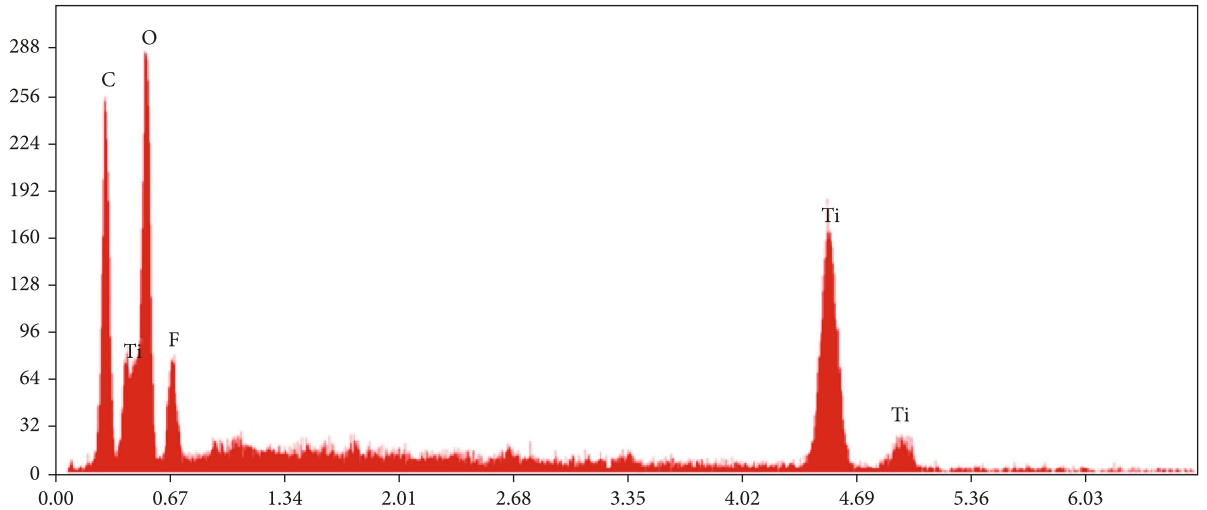

Figure 4: EDS spectrum of TiO_2 obtained at 50 V for 60 minutes in glycerol-distilled water (92 : 8% *v*/*v*) and NH_4F 0.4 M.

scanning electron microscope TESCAN VEGA 3 was used. SEM top images and cross-sections of nanotube arrays produced in glycerol-distilled water (92 : 8% *v*/*v*) and NH_4F (0.4 M) for 60 min at different anodizing potentials are given in Figure 2.

The electrochemical anodization of titanium under these conditions leads to the formation of an ordered nanotubular array on the titanium surface. For the anodized sample at 30 V, there are areas where the oxide formed is compact. In addition, other areas have an ordered distribution of medium-sized nanotubes of about 59 nm in diameter. For voltages above 30 V, the surface of the samples is made up of neat TiO_2 nanotubes. The average diameters of the nanotubes are about 80 nm and 128 nm for an applied voltage of 40 V and 60 V, respectively.

In addition, the lengths of the nanotubes were measured by scanning electron microscope observation of cross-sections of the films. The result showed that the length of the TiO_2 nanotube obtained on the surface of the titanium metal increases with the increasing anodization potential to reach approximately 1.5 μm at 60 V.

Figure 3 shows the evolution of nanotubular internal diameter as a function of the anodizing voltage. It is clearly seen that the nanotube diameter increases linearly with the

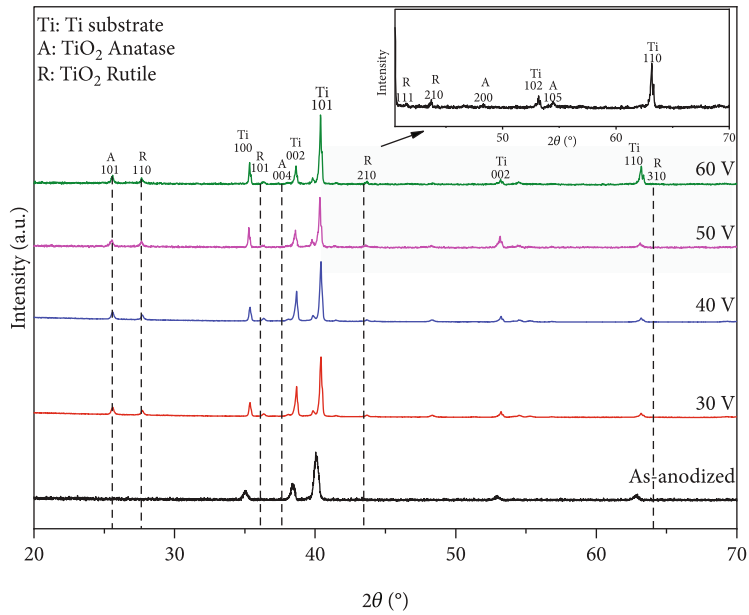

Figure 5: XRD spectra of samples anodized at different anodization potentials in glycerol-distilled water (92 : 8% *v*/*v*) and NH_4F 0.4 M.

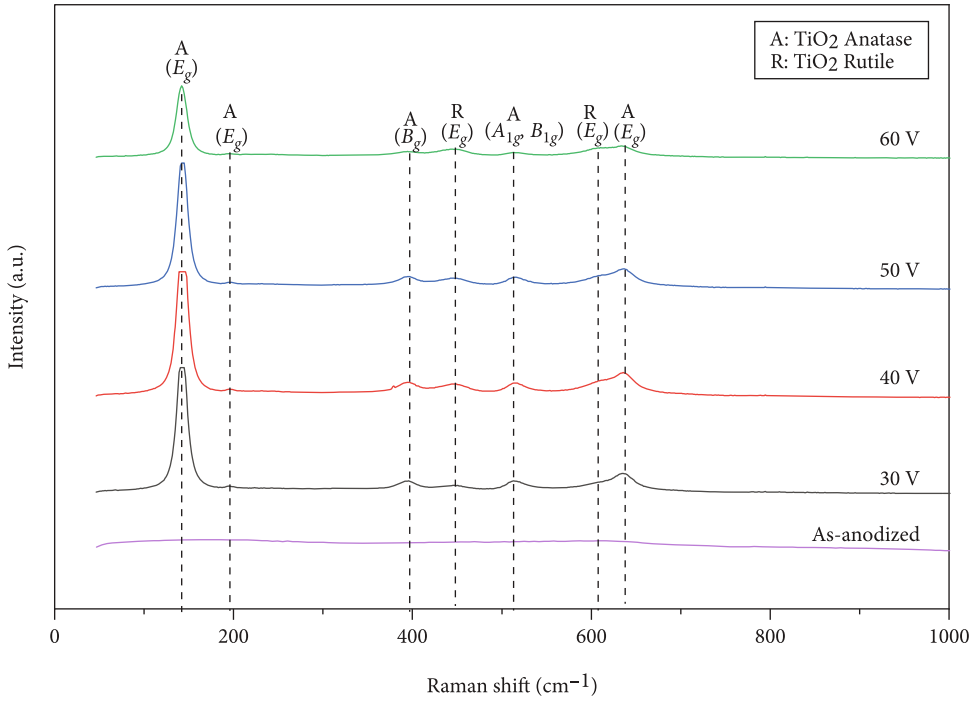

Figure 6: Raman spectra of anodized simples at different anodization potentials in glycerol-distilled water (92 : 8% *v*/*v*) and NH_4F 0.4 M.

anodizing potential with a good correlation coefficient R^2 that is close to 1 (0.97). It should be noted that for a potential of 30 V, the internal diameter of the nanotubes is about 59 nm, while it reached 128 nm for a potential of 60 V.

3.3. Composition Analysis by EDX. For the elemental characterization of the obtained nanotubular layers, energy-dispersive X-ray analysis is conducted using an acceleration voltage of 10 kV. The characteristics of the emitted X-rays from the anodized substrate produced at different conditions are presented in Figure 4. The EDX spectrum indicates the presence of the Tik_α peak at 4.58 eV and O peaks at 0.5 eV, as well as F and C peaks in the anodized sample. The obtained percentages of Ti (26.5 at%) and O (41.4 at%) yield a Ti/O ratio of about 0.5 indicating that the structure of the formed oxide is TiO_2 with the

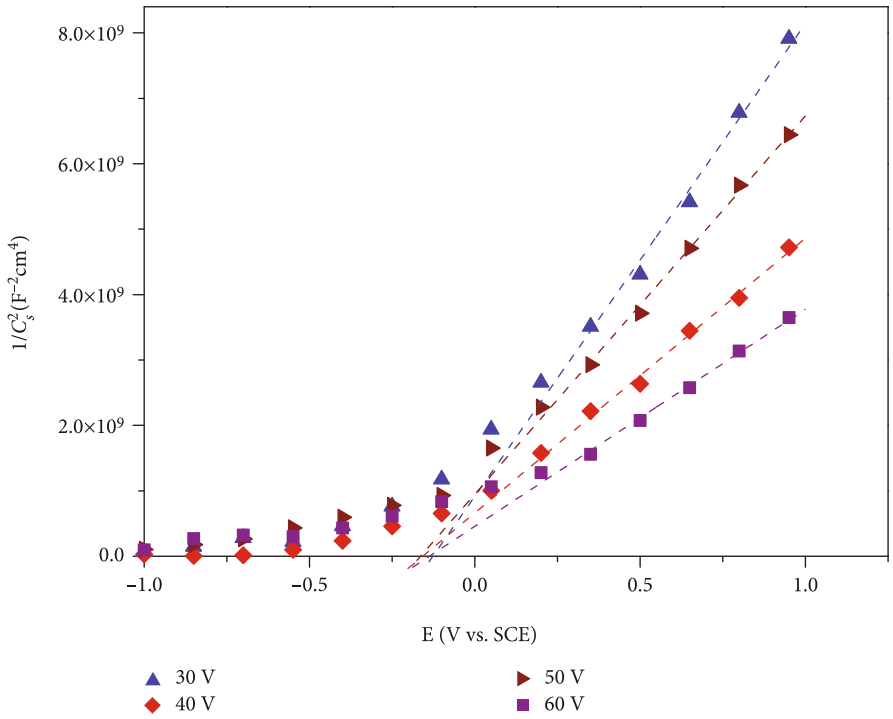

Figure 7: Mott-Schottky plots obtained for the formed nanotubularTiO_2 layers in 0.1 M Na_2SO_4 solution.

presence of fluorine that arises from the solution during the anodization process [35] and carbon which comes from the metallization process using graphite.

3.4. XRD Structural Characterization. The crystal phases of as-prepared and annealed samples were identified by XRD using Cu Kα radiation. As show in Figure 5, the formed TiO_2 nanotubular film consists of a mixture of anatase and rutile phases. The anatase phase was identified from the peaks at ca. 25.03°, 48.05°, 54.85°, and 55.30° characteristic of the planes (101), (200), (105), and (211), respectively, according to JCPDS file no. 21-1272. In addition, the rutile phase is revealed by peaks at 27.4°, 36.07°, 41°, 43.6°, and 56.9°, corresponding to planes (110), (101), (110), (111), (210), and (220) (JCPDS card no. 21-1276), respectively. XRD spectra of annealed oxides reveal that TiO_2 peaks become more intense when the anodizing potential increases.

The crystallite size is an important factor to determine the stability of nanotubular TiO_2 crystalline phases [1, 36]. The average crystallite size of nanotubular TiO_2 samples is calculated using the Scherrer equation $D = 0.9\lambda/\beta\text{Cos}\theta$, where D is the grain size, λ (1.548 Å) is the wavelength of X-ray radiation used, θ is the Bragg diffraction angle obtained from XRD peak, and β is the full width at half maximum of the diffraction peak [37]. Using the width of the (101) peak for anatase and the width of the (110) peak for rutile, crystallite sizes were obtained in the ranges 7.3 to 8.5 nm and 8.2 to 9.7 nm for anatase and rutile phases, respectively.

On the other hand, the phase composition of TiO_2 has a crucial impact on the photocatalytic activity. The effect of the anatase/rutile ratio is discussed in many controversial works. It is reported that a mixture of anatase and rutile phases was found suitable for photocatalytic oxidation of organic pollutants in water [38]. Nevertheless, Tayade et al. [39] suggested that only the anatase phase has attracted considerable attention as a photocatalyst for the chemical treatment of organic pollutants. In our conditions, the relative amounts of anatase and rutile were estimated at 82% and 18%, respectively. This result is similar to that for the commercial TiO_2, Degussa P25, which exhibits a strong photocatalytic activity and has an anatase-rutile mass fraction of 80 : 20.

Table 1: N_D and E_{FB} of anodized samples at different potentials.

Tension (V)	E_{FB} (V/SCE)	$N_D \times 10^{-17}$ (cm^{-3})
30	-0.13	1.95
40	-0.16	3.37
50	-0.10	2.45
60	-0.14	4.25

3.5. Structural Characterization by Raman Microscopy. The TiO_2 films obtained at different anodizing voltages were also characterized by Raman spectroscopy after thermal annealing at 600°C. Figure 6 shows the Raman spectra of the different anodized samples at different anodization potentials in a glycerol-distilled water mixture.

For the as-anodized sample, we noticed the absence of Raman peaks indicating the amorphous nature of the formed oxide [40]. However, the Raman spectra of all

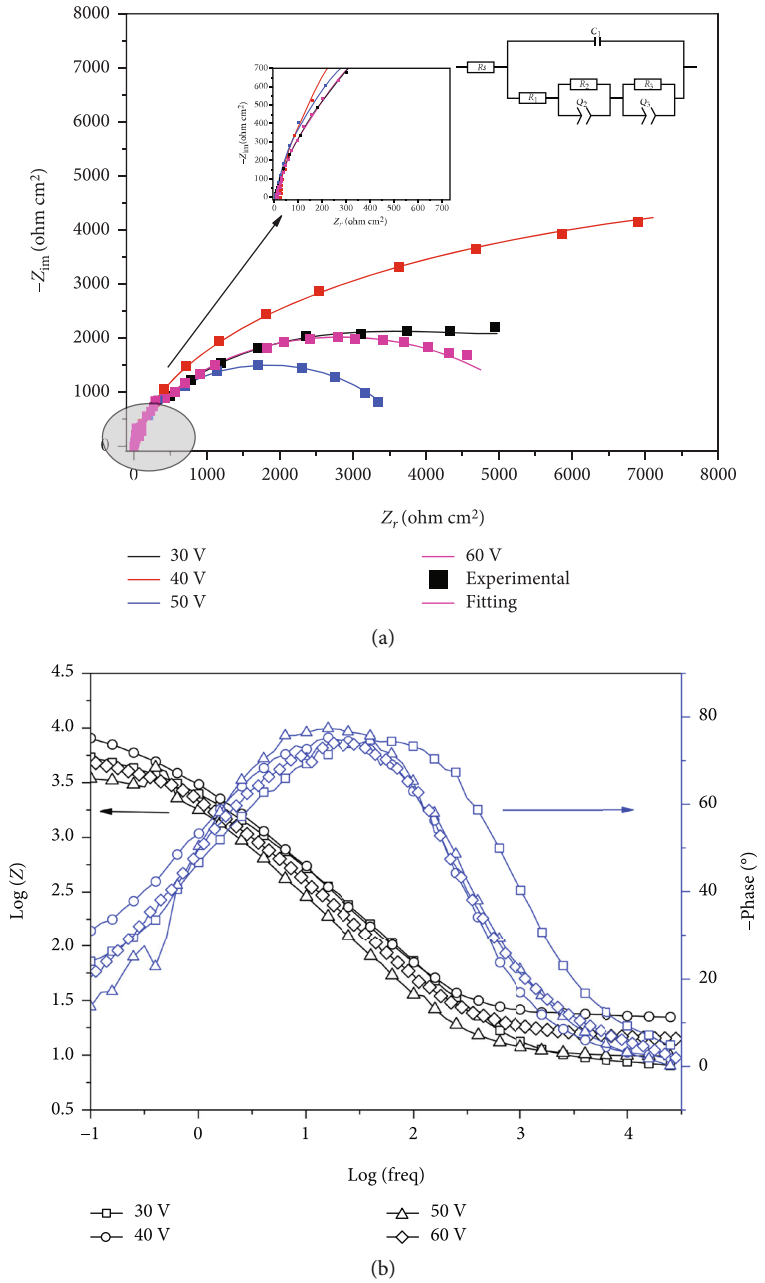

FIGURE 8: Diagrams of the EIS data obtained for the TiO_2: (a) Nyquist representations and (b) Bode representations. The equivalent circuit used to fit the experimental impedance spectra is inserted into (a).

annealed samples depict a similar trend and show a very intense band at 143 cm^{-1} and four others at 195, 394, 515, and 637 cm^{-1}. These bands can be attributed to the vibrational modes $E_{g(1)}$,$E_{g(2)}$,B_{1g},A_{1g}, orB_{1g}(superposition ofA_{1g}andB_{1g}), andE_g of anatase, respectively. The observed bands confirm the predominance of anatase as the crystalline phase in the structure [41]. However, peaks of about 447 and 619 cm^{-1} indicate the presence of a certain amount of rutile and their intensities increase with the anodizing potential. These vibration modes are shifted by 2 to 4 cm^{-1} due to the variation in grain size and stoichiometric defects present in TiO_2 structures as reported by Bassi et al. [42]. These structural observations are in good agreement with the XRD analysis.

3.6. Mott-Schottky (MS) Analysis. Electrochemical capacitance measurements were carried out to characterize the semiconductor nature of the films and to determine the donor density N_D of the formed TiO_2 layers, as well as to estimate the flat band potential (E_{FB}) of the anodized samples at different potentials. MS analysis was performed in Na_2SO_4 0.1 M at 1 kHz in the potential range of -1 to 1 V/SCE. Figure 7 shows the variation of $1/C_s^2$ as a function of potential E (V/SCE).

Table 2: Parameters obtained by fitting the impedance spectra of the anodized samples at different applied potentials.

	R_s ($\Omega \times cm^2$)	C_1 ($\mu F/m^2$)	R_1 ($\Omega \times cm^2$)	Q_2 ($\mu F \times s^{(a-1)}$)	a_2	R_2 ($k\Omega \times cm^2$)	Q_3 ($mF \times s^{(a-1)}$)	a_3	R_3 ($k\Omega \times cm^2$)
30 V	7.74	19.9	127.20	86.18	0.44	4.38	0.55	0.97	9.35
40 V	23.08	23.76	25.63	95.42	0.45	1.31	0.11	0.70	21.76
50 V	10.13	47.89	7.63	56.64	0.29	1.02	0.23	0.60	5.67
60 V	14.99	23.52	2.76	76.49	0.56	4.31	0.92	0.68	19.65

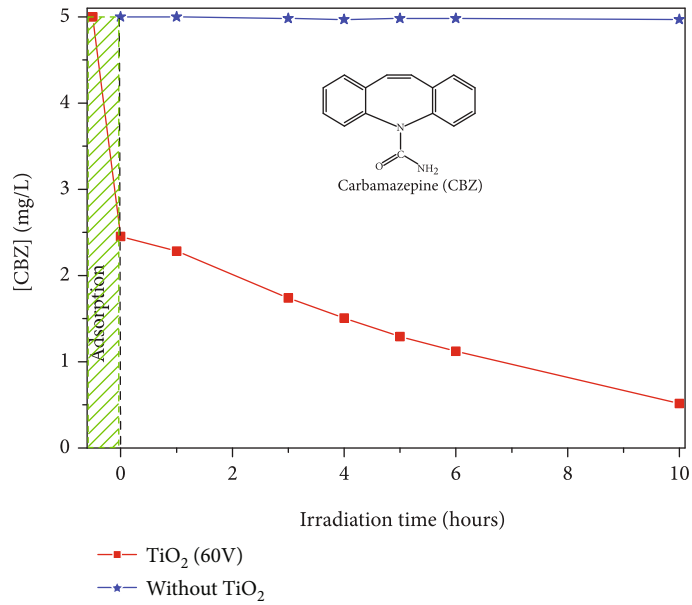

Figure 9: Photocatalytic activity of TiO_2 nanotubular- (formed at 60 V and annealed at 600°C) simulated sunlight irradiation (300 W).

As shown in Figure 7, a quasilinear behavior of the variation of $1/(C_s^2)$ as a function of the potential was observed. All curves have a positive slope corresponding to an n-type semiconductor [43]. The parameters N_D and E_{FB} can be determined from the slope of the linear regions in the Mott-Schottky plot and its intersection with the x-axis, respectively, according to the Mott-Schottky relationship:

$$\frac{1}{C_S^2} = \frac{2}{\varepsilon_0 \varepsilon_S e N_D}\left(E - E_{FB} - \frac{kT}{e}\right), \quad (3)$$

where C_S is the space charge layer capacitance, e the electron charge ($1.60\,10^{-19}$ C), ε_0 the permittivity of free space ($8.85\,10^{-14}$ F cm^{-1}), ε_S the dielectric constant of TiO_2 which is assumed to be 100 F cm^{-1} [44], E the applied potential, k the Boltzmann constant ($1.38\,10^{23}$ J K^{-1}), and T the absolute temperature. The values of the N_D and E_{FB} of the different samples are summarized in Table 1.

Table 1 shows clearly that the N_D values increase with anodizing potential, and the values obtained are in the order of 10^{17} cm^{-3}. The N_D values obtained are in good agreement with those reported in the literature for nanotubular TiO_2 [45]. Generally, the growth of the anodized oxide films is always nonstoichiometric with an excess/deficiency of metal cations or oxygen anions [40]. According to the Point Defect Model (PDM), the n-type semiconductor behavior of an anodic passive film indicates that the defects in all samples are due to the oxygen deficiencies and/or interstitial titanium ions [46]. Somehow, Peng [47] reported that the predominance of oxygen deficiency is due to the low formation energy of oxygen vacancy compared to the interstitial titanium.

3.7. Electrochemical Impedance Spectroscopy. Electrochemical impedance spectroscopy (EIS) technique was used to study the electrochemical behavior of the interface of TiO_2 nanotubular film. Figures 8(a) and 8(b) present the Nyquist and Bode diagrams of the EIS data obtained for the TiO_2 films with their fitting adjustments obtained using EC-Lab software with the suggested equivalent circuit (inset in Figure 8(a)).

The Bode diagrams of Figure 8(b) reveal the presence of more than two time constants in the lower and intermediate frequency ranges. This behavior can be attributed to the presence of an inner compact layer and an outer porous TiO_2 nanotube layer [48]. In addition, the decrease in phase angles at a high frequency is related to the porous nature of the outer layer [35]. At intermediate frequencies, the spectrum log $|z|$ vs. log(freq) is a straight line with a slope ranging from -0.78 to -0.88 that exhibits capacitive behavior.

The Nyquist diagrams shown in Figure 8(a) represent incomplete semicircles at low frequencies. Different equivalent circuits have been proposed in the literature to model the TiO_2/electrolyte interface [40, 49]. In our case, Nyquist spectra are adjusted using the following equivalent electrical circuit as $R_s + C_1/(R_1 + Q_2/R_2 + Q_3/R_3)$.

The proposed equivalent circuit takes into account the different time constants. The TiO_2/electrolyte interface can be represented by the Helmholtz capacitance (C_1). As shown in the equivalent circuit, this capacitance (C_1) is in parallel with a resistance coupled to the constant phase element (R_2/Q_2) and (R_3/Q_3), corresponding, respectively, to the porous (outer) and barrier (inner) layer. Constant phase elements (Q) are used to take into account the surface heterogeneity, nonideality of capacitance, and frequency dispersion [50, 51]. The values of the circuit elements are summarized in Table 2.

For all the studied potentials, the calculated R_s and C_1 parameters vary slightly compared to the other parameters. It is interesting to note that the resistance of the barrier layer R_3 is higher than R_2 of the nanotubes. The a_2 values of the tubular layers are ranging from 0.29 to 0.56, while the a_3 values of the barrier layers are between 0.60 and 0.97 for all samples which can be associated with a distribution of relaxation times due to the heterogeneities at the surface. The a_2 values indicate that the tubular layers of all samples have a nonideal capacitive behavior. Values in the order of 0.30 and 0.50 have been reported in the literature for porous materials [52].

3.8. Photocatalytic Activity. To value the photocatalytic activity of nanoporous TiO_2 formed in our conditions, the TiO_2 nanotube arrays formed at 60 V and annealed at 600°C are evaluated for the degradation of a pharmaceutical pollutant known for its photochemical stability, carbamazepine (CBZ) [49]. Figure 9 shows the degradation curve of CBZ in an aqueous solution with an initial concentration of 5 ppm in the presence of the TiO_2 nanotubes and under simulated sunlight irradiation (300 W). As it can be clearly observed, the anodized TiO_2 in these conditions can effectively degrade 96% of CBZ within 10 h of irradiation. This may be due to their large surface area the TiO_2 nanotubes and to their crystalline size and phase composition. Under these anodization conditions, TiO_2 nanotube arrays were characterized by a pore diameter of 128 nm, a tube depth of 1.5 μm, and a maximum donor charge of about 4.25 10^{17} cm^{-3}. With this tube length, in combination with minimal radial dimensions, the incident illumination can be effectively captured near the surface of the nanotubes, providing facile separation of a photogenerated charge. Our results are promising, and further work is underway to study the influence of other parameters on the photocatalytic activity of titanium dioxide nanotubes.

4. Conclusion

The electrochemical anodizing method was used to produce amorphous TiO_2 nanotubes converted by annealing into crystalline nanotubes. The nanotubes of significantly different diameters were obtained in a voltage range from 30 V to 60 V. The variation in anodizing voltage did not modify the chemical composition of the TiO_2. In addition, their crystalline structure shows the presence of a mixture of anatase and rutile phases. The electrochemical study reveals that the oxide formed under these conditions is an n-type semiconductor with a donor density on the order of 10^{17} cm^{-3}. Our results are promising, and further work is underway to study of the photocatalytic properties of the produced titanium oxide nanotubes.

Data Availability

The data used to support the findings of this study are available from the corresponding author upon request.

Additional Points

Highlights. (i) Nanotubular titanium dioxide (TiO_2) array was produced by the anodization method; (ii) applied potential significantly affects the nanotube diameter; (iii) the anodic TiO_2 was analyzed by SEM, XRD, Raman spectra, Mott-Schottky analysis, and EIS measurements; (iv) photocatalytic degradation of a pharmaceutical pollutant was achieved.

Conflicts of Interest

The authors declare that they have no conflicts of interest regarding the publication of this paper.

Acknowledgments

The authors are grateful to the Centre of Analysis and Characterization (CAC) of the Faculty of Sciences Semlalia in Marrakesh, Morocco, for help in characterization, and the National Center for Scientific and Technical Research (CNRST) in Rabat for its financial support.

References

[1] H. Wu and Z. Zhang, "Photoelectrochemical water splitting and simultaneous photoelectrocatalytic degradation of organic pollutant on highly smooth and ordered TiO_2 nanotube arrays," *Journal of Solid State Chemistry*, vol. 184, no. 12, pp. 3202–3207, 2011.

[2] T. S. Natarajan, K. Natarajan, H. C. Bajaj, and R. J. Tayade, "Energy efficient UV-LED source and TiO_2 Nanotube array-based reactor for photocatalytic application," *Industrial and Engineering Chemistry Research*, vol. 50, no. 13, pp. 7753–7762, 2011.

[3] S. Rafqah, P. Wong-Wah-Chung, S. Nelieu, J. Einhorn, and M. Sarakha, "Phototransformation of triclosan in the presence of TiO2 in aqueous suspension: mechanistic approach," *Applied Catalysis B: Environmental*, vol. 66, no. 1–2, pp. 119–125, 2006.

[4] J.-H. Xu and F. Shiraishi, "Photocatalytic decomposition of acetaldehyde in air over titanium dioxide," *Journal of Chemical Technology and Biotechnology*, vol. 74, no. 11, pp. 1096–1100, 1999.

[5] H. Park, W.-R. Kim, H.-T. Jeong, J.-J. Lee, H.-G. Kim, and W.-Y. Choi, "Fabrication of dye-sensitized solar cells by transplanting highly ordered TiO_2 nanotube arrays," *Solar Energy Materials & Solar Cells*, vol. 95, no. 1, pp. 184–189, 2011.

[6] H. H. Park, K. S. Kim, W. Y. Jeon et al., "Bioactive and electrochemical characterization of TiO_2 nanotubes on titanium via

anodic oxidation," *Electrochimica Acta*, vol. 55, no. 20, pp. 6109–6114, 2010.

[7] S. M. H. Al-jawad, "Effect of doping on structural and electrical properties of titanium dioxide (TiO_2) thin films for gas sensor," *International Journal of Scientific & Engineering Research*, vol. 5, no. 1, pp. 2171–2176, 2014.

[8] M. Salari, S. H. Aboutalebi, K. Konstantinov, and H. K. Liu, "A highly ordered titania nanotube array as a supercapacitor electrode," *Physical Chemistry Chemical Physics*, vol. 13, no. 11, pp. 5038–5041, 2011.

[9] J. M. Macak, A. Ghicov, K. Yasuda et al., "TiO_2 nanotubes: self-organized electrochemical formation, properties and applications," *Current Opinion in Solid State & Materials Science*, vol. 11, no. 1–2, pp. 3–18, 2007.

[10] M. Abdennouri, R. Elmoubarki, A. Elmhammedi et al., "Influence of tungsten on the anatase-rutile phase transition of sol-gel synthesized TiO_2 and on its activity in the photocatalytic degradation of pesticides," *Journal of Materials and Environmental Science*, vol. 4, no. 6, pp. 953–960, 2013.

[11] L. Korösi and I. Dékány, "Preparation and investigation of structural and photocatalytic properties of phosphate modified titanium dioxide," *Colloids and Surfaces A: Physicochemical and Engineering Aspects*, vol. 280, no. 1–3, pp. 146–154, 2006.

[12] D. Gong, O. K. Varghese, W. Hu et al., "Titanium oxide nanotube arrays prepared by anodic oxidation," *Journal of Materials Research*, vol. 16, no. 12, pp. 3331–3334, 2001.

[13] N. Li, Y. Li, W. Li, S. Ji, and P. Jin, "One-step hydrothermal synthesis of TiO_2@MoO_3 Core–Shell nanomaterial: microstructure, growth mechanism, and improved photochromic property," *Journal of Physical Chemistry C*, vol. 120, no. 6, pp. 3341–3349, 2016.

[14] Y. X. TANG, J. TAO, Y. Y. ZHANG, T. WU, H. J. TAO, and Y. R. ZHU, "Preparation of TiO_2 nanotube on glass by anodization of Ti films at room temperature," *Transactions of the Nonferrous Metals Society of China*, vol. 19, no. 1, pp. 192–198, 2009.

[15] Y. Fu and A. Mo, "A review on the electrochemically self-organized titania nanotube arrays: synthesis, modifications, and biomedical applications," *Nanoscale Research Letters*, vol. 13, no. 1, p. 187, 2018.

[16] M. Sun, D. Yu, L. Lu, W. Ma, Y. Song, and X. Zhu, "Effective approach to strengthening TiO_2 nanotube arrays by using double or triple reinforcements," *Applied Surface Science*, vol. 346, pp. 172–176, 2015.

[17] S. -y. Zhang, D. L. Yu, D. D. Li et al., "Forming process of anodic TiO_2 Nanotubes under a preformed compact surface layer," *Journal of The Electrochemical Society*, vol. 161, no. 10, pp. E135–E141, 2014.

[18] Z. Lockman, S. Sreekantan, S. Ismail, L. Schmidt-Mende, and J. L. MacManus-Driscoll, "Influence of anodisation voltage on the dimension of titania nanotubes," *Journal of Alloys and Compounds*, vol. 503, no. 2, pp. 359–364, 2010.

[19] S. Zhang, S. Zhang, P. Xu, and K. Liang, "Effect of anodization parameters on the surface morphology and photoelectrochemical properties of TiO_2 nanotubes," *International Journal of Electrochemical Science*, vol. 12, no. 11, pp. 10714–10725, 2017.

[20] J. Chen, J. Lin, and X. Chen, "Self-assembled TiO_2 nanotube arrays with U-shaped profile by controlling anodization temperature," *Journal of Nanomaterials*, vol. 2010, Article ID 753253, 4 pages, 2010.

[21] K. M. Deen, A. Farooq, M. A. Raza, and W. Haider, "Effect of electrolyte composition on TiO_2 nanotubular structure formation and its electrochemical evaluation," *Electrochimica Acta*, vol. 117, pp. 329–335, 2014.

[22] D. Regonini and F. J. Clemens, "Anodized TiO_2 nanotubes: effect of anodizing time on film length, morphology and photoelectrochemical properties," *Materials Letters*, vol. 142, pp. 97–101, 2015.

[23] A. Valota, P. Skeldon, M. Curioni et al., "Influence of water content on nanotubular anodic titania formed in fluoride/glycerol electrolytes," *Electrochimica Acta*, vol. 54, no. 18, pp. 4321–4327, 2009.

[24] M. Kulkarni, "Influence of anodization parameters on morphology of TiO_2 nanostructured surfaces," *Advanced Materials Letters*, vol. 7, no. 1, pp. 23–28, 2016.

[25] B.-G. LEE, J.-W. CHOI, S.-E. LEE, Y.-S. JEONG, H.-J. OH, and C.-S. CHI, "Formation behavior of anodic TiO_2 nanotubes in fluoride containing electrolytes," *Transactions of the Nonferrous Metals Society of China*, vol. 19, no. 4, pp. 842–845, 2009.

[26] M. Paulose, S. Yoriya, H. E. Prakasam et al., "Anodic growth of highly ordered TiO_2Nanotube arrays to 134 μm in length," *The Journal of Physical Chemistry. B*, vol. 110, no. 33, pp. 16179–16184, 2006.

[27] J. M. Macák, H. Tsuchiya, and P. Schmuki, "High-aspect-ratio TiO_2 nanotubes by anodization of titanium," *Angewandte Chemie International Edition*, vol. 44, no. 14, pp. 2100–2102, 2005.

[28] A. Jaroenworaluck, D. Regonini, C. R. Bowen, R. Stevens, and D. Allsopp, "Macro, micro and nanostructure of TiO_2 anodised films prepared in a fluorine-containing electrolyte," *Journal of Materials Science*, vol. 42, no. 16, pp. 6729–6734, 2007.

[29] S. P. Albu, A. Ghicov, J. M. Macak, and P. Schmuki, "250 μm long anodic TiO_2 nanotubes with hexagonal self-ordering," *Physica Status Solidi (RRL) – Rapid Research Letters*, vol. 1, no. 2, pp. 65–67, 2007.

[30] S. Sreekantan, K. A. Saharudin, and L. C. Wei, "Formation of TiO_2 nanotubes via anodization and potential applications for photocatalysts, biomedical materials, and photoelectrochemical cell," *IOP Conference Series: Materials Science and Engineering*, vol. 21, no. 1, 2011.

[31] M. Khadiri, M. Elyaagoubi, R. Idouhli et al., "Electrochemical study of anodized titanium in phosphoric acid," *Advances in Materials Science and Engineering*, vol. 2020, 11 pages, 2020.

[32] H. Shi, "Formation mechanism of anodic TiO2 nanotubes," in *Proceedings of the 2017 2nd International Conference on Materials Science, Machinery and Energy Engineering (MSMEE 2017)*, vol. 123, pp. 785–788, Dalian, China, 2017.

[33] H. Yoo, M. Kim, Y.-T. Kim, K. Lee, and J. Choi, "Catalyst-doped anodic TiO_2 nanotubes: binder-free electrodes for (photo)-electrochemical reactions," *Catalysts*, vol. 8, no. 11, p. 555, 2018.

[34] D. Regonini, C. R. Bowen, A. Jaroenworaluck, and R. Stevens, "A review of growth mechanism, structure and crystallinity of anodized TiO_2 nanotubes," *Materials Science and Engineering: R: Reports*, vol. 74, no. 12, pp. 377–406, 2013.

[35] J. Macák, *Growth of Anodic Self-Organized Titanium Dioxide Nanotube Layers*, Universität Erlangen-Nürnberg, 2008.

[36] H. Wu and Z. Zhang, "High photoelectrochemical water splitting performance on nitrogen doped double-wall TiO_2 nanotube array electrodes," *International Journal of Hydrogen Energy*, vol. 36, no. 21, pp. 13481–13487, 2011.

[37] V. Likodimos, C. Han, M. Pelaez et al., "Anion-doped TiO_2 nanocatalysts for water purification under visible light," *Industrial and Engineering Chemistry Research*, vol. 52, no. 39, pp. 13957–13964, 2013.

[38] S. Bakardjieva, J. Šubrt, V. Štengl, M. J. Dianez, and M. J. Sayagues, "Photoactivity of anatase-rutile TiO_2 nanocrystalline mixtures obtained by heat treatment of homogeneously precipitated anatase," *Applied Catalysis B: Environmental*, vol. 58, no. 3–4, pp. 193–202, 2005.

[39] R. J. Tayade, P. K. Surolia, R. G. Kulkarni, and R. V. Jasra, "Photocatalytic degradation of dyes and organic contaminants in water using nanocrystalline anatase and rutile TiO2," *Science and Technology of Advanced Materials*, vol. 8, no. 6, pp. 455–462, 2007.

[40] B. Munirathinam and L. Neelakantan, "Titania nanotubes from weak organic acid electrolyte: fabrication, characterization and oxide film properties," *Materials Science and Engineering: C*, vol. 49, pp. 567–578, 2015.

[41] P. M. Dziewoński and M. Grzeszczuk, "Deposition of thin TiO_2 layers on platinum by means of cyclic voltammetry of selected complex Ti(IV) media leading to anatase," *Electrochimica Acta*, vol. 54, no. 16, pp. 4045–4055, 2009.

[42] A. L. Bassi, D. Cattaneo, V. Russo et al., "Raman spectroscopy characterization of titania nanoparticles produced by flame pyrolysis: the influence of size and stoichiometry," *Journal of Applied Physics*, vol. 98, no. 7, 2005.

[43] G. Rahman and O. Joo, "Photoelectrochemical water splitting at nanostructured α-Fe_2O_3 electrodes," *International Journal of Hydrogen Energy*, vol. 37, no. 19, pp. 13989–13997, 2012.

[44] P. Pu, H. Cachet, and E. M. M. Sutter, "Electrochemical impedance spectroscopy to study photo-induced effects on self-organized TiO_2 nanotube arrays," *Electrochimica Acta*, vol. 55, no. 20, pp. 5938–5946, 2010.

[45] S. Palmas, A. da Pozzo, M. Mascia et al., "Effect of the preparation conditions on the performance of TiO_2 nanotube arrays obtained by electrochemical oxidation," *International Journal of Hydrogen Energy*, vol. 36, no. 15, pp. 8894–8901, 2011.

[46] Z. Jiang, X. Dai, and H. Middleton, "Investigation on passivity of titanium under steady-state conditions in acidic solutions," *Materials Chemistry and Physics*, vol. 126, no. 3, pp. 859–865, 2011.

[47] H. Peng, "First-principles study of native defects in rutile TiO_2," *Physics Letters A*, vol. 372, no. 9, pp. 1527–1530, 2008.

[48] S. Palmas, A. M. Polcaro, J. R. Ruiz, A. Da Pozzo, M. Mascia, and A. Vacca, "TiO_2 photoanodes for electrically enhanced water splitting," *International Journal of Hydrogen Energy*, vol. 35, no. 13, pp. 6561–6570, 2010.

[49] A. Morais, C. Longo, J. R. Araujo, M. Barroso, J. R. Durrant, and A. F. Nogueira, "Nanocrystalline anatase TiO_2/reduced graphene oxide composite films as photoanodes for photoelectrochemical water splitting studies: the role of reduced graphene oxide," *Physical Chemistry Chemical Physics*, vol. 18, no. 4, pp. 2608–2616, 2016.

[50] B. Lucas-Granados, R. Sánchez-Tovar, R. M. Fernández-Domene, and J. García-Antón, "Iron oxide nanostructures for photoelectrochemical applications: effect of applied potential during Fe anodization," *Journal of Industrial and Engineering Chemistry*, vol. 70, pp. 234–242, 2019.

[51] A. G. Muñoz, "Semiconducting properties of self-organized TiO2 nanotubes," *Electrochimica Acta*, vol. 52, no. 12, pp. 4167–4176, 2007.

[52] D. Qu, "Application of a.c. impedance technique to the study of the proton diffusion process in the porous MnO_2 electrode," *Electrochimica Acta*, vol. 48, no. 12, pp. 1675–1684, 2003.